

Towards Visual Query Segmentation in the Wild

Bing Fan*, Minghao Li*, Hanzhi Zhang*, Shaohua Dong
Naga Prudhvi Mareedu, Weishi Shi, Yunhe Feng, Yan Huang, and Heng Fan

Department of Computer Science and Engineering, University of North Texas

Abstract. In this paper, we introduce *visual query segmentation* (VQS), a new paradigm of visual query localization (VQL) that aims to segment *all pixel-level* occurrences of an object of interest in an *untrimmed* video, given an external visual query. Compared to existing VQL locating only the last appearance of a target using bounding boxes, VQS enables more comprehensive (*i.e.*, *all* object occurrences) and precise (*i.e.*, *pixel-level* masks) localization, making it more practical for real-world scenarios. To foster research on this task, we present VQS-4K, a large-scale benchmark dedicated to VQS. Specifically, VQS-4K contains 4,111 videos with more than 1.3 million frames, and covers a diverse set of 222 object categories. Each video is paired with a visual query defined by a frame *outside* search video and its target mask, and annotated with spatial-temporal masklets corresponding to the queried target. To ensure high quality, all videos in VQS-4K are manually labeled with meticulous inspection and iterative refinement. To the best of our knowledge, VQS-4K is the *first* benchmark specifically designed for VQS. Furthermore, to stimulate future research, we present a simple yet effective method, named VQ-SAM, which extends SAM 2 by leveraging target-specific and background distractor cues from the video to progressively evolve the memory through a novel multi-stage framework with an adaptive memory generation (AMG) module for VQS, significantly improving the performance. In our extensive experiments on VQS-4K, VQ-SAM achieves promising results and surpasses all existing approaches, demonstrating its effectiveness. With the proposed VQS-4K and VQ-SAM, we expect to go beyond current VQL paradigm and inspire more future research and practical applications on VQS. Our benchmark, code, and results will be made publicly available.

Keywords: Visual Query Segmentation (VQS) · Benchmark

1 Introduction

Visual query localization (VQL) aims to search and locate an object of interest in *space* and *time* from an *untrimmed* video, given a visual query obtained outside the search video. As a fundamental task in computer vision, it has many crucial applications such as surveillance, robotics, and video object retrieval and editing.

Currently, the research of VQL mainly focuses on locating the *last* appearance of a target in a video [9] (see Fig. 1 (a)). Despite significant progress [2, 8, 11–13,

*Equal contribution

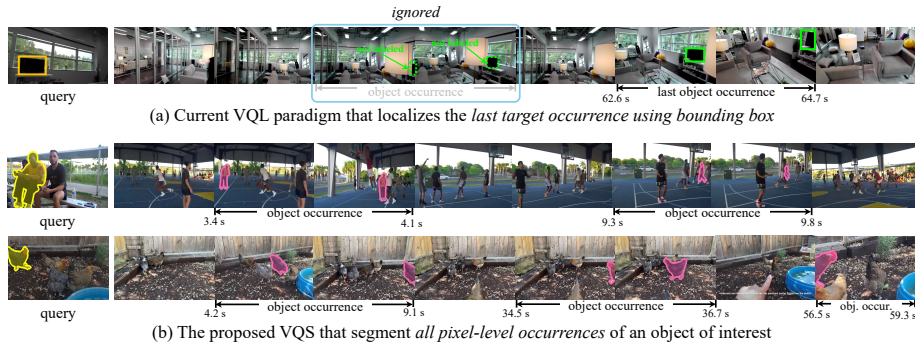


Fig. 1: Comparison of existing VQL paradigm that localizes the last target occurrence using bounding box (a) and our VQS segmenting all pixel-level occurrences of an object (b).

[18, 31], this VQL paradigm remains *insufficient* for many real-world scenarios involving multiple target occurrences, such as visual surveillance and video object retrieval, in which knowing *all* target occurrences, rather than only the last one, is essential for comprehensive video understanding. In addition, in the current VQL setting, objects are often represented using *bounding boxes* (see again Fig. 1 (a)). While simple, this representation tends to introduce noise into objects, and thus limits precise spatial localization of targets, hindering its applicability to downstream tasks demanding accurate target localization such as video editing.

To mitigate the above issues, we introduce *visual query segmentation* (VQS), a new VQL paradigm that aims to segment *all pixel-level* occurrences of a target of interest within an untrimmed video, given a visual query (see Fig. 1 (b)). In comparison with existing VQL [9], VQS enables both *comprehensive* localization by capturing *all* target occurrences throughout a video and *precise* localization by representing objects with *pixel-level* masks, making it more suitable in real-world applications. It is worth noting that, despite sharing certain similarities to video object segmentation (VOS) [6, 10, 22, 32, 34], VQS fundamentally differs. Unlike VOS where the reference target is sampled from the first frame *within* the video, the query in VQS is sourced from an image frame *outside* the search video. This makes localization in VQS more challenging, as there may be no exact visual match and close frames for the queried object. Besides, VOS typically operates at *frame-level* via sequential propagation in a trimmed video, while VQS performs *video-level* global search across an untrimmed video, which makes it a *needle-in-the-haystack* problem and requires a model to identify and segment sparse and intermittent target occurrences amidst substantial background distractors.

Considering the lack of a dedicated benchmark for studying VQS, we propose VQS-4K, a large-scale dataset for this task. Specifically, VQS-4K comprises 4,111 videos with over 1.3 million frames, spanning 222 object categories across diverse in-the-wild contexts. Each sequence is paired with a visual query that is sampled from a frame outside the search video, together with a mask indicating the target of interest, and is annotated with a varying number of spatio-temporal masklets that correspond to the queried target. To ensure the high quality of our VQS-4K, all mask annotations in each sequence are manually annotated with meticulous

inspection and undergo multi-round careful refinement as necessary. To our best knowledge, VQS-4K is to date the *first* publicly available benchmark specifically designed for VQS. Fig. 1 (b) demonstrates several example sequences in VQS-4K.

Furthermore, to encourage future research, we introduce a simple yet effective model for VQS, termed VQ-SAM, by extending SAM 2 [25]. Its core is to leverage both target-specific information and background distractor cues to progressively evolve the memory for VQS. Concretely, VQ-SAM is formulated as a multi-stage architecture. In each stage, we first generate potential object masks from a video using current memory. With these masks and confidence scores, we then select a few top target and distractor regions to extract the target-specific and distractor features respectively, similar to [28]. These features, together with initial memory from the visual query, are utilized to generate the new memory. Considering that different features may contribute unequally in memory, we propose an adaptive memory generation (AMG) module that learns importance weights for different feature types and integrates them accordingly to form memory. By incorporating the target-specific features, the newly evolved memory can better handle target variations in videos. Besides, leveraging distractor features enables more reliable discrimination between the target and the background. In VQ-SAM, the memory generated in one stage is used in the next stage to produce more accurate target-specific and background distractor features, which are then used to further evolve the memory. Through this progressive process, the memory is gradually improved in VQ-SAM, resulting in better localization and segmentation in the final stage.

It is important to note that, despite sharing a similar spirit with [8] in adopting a progressive framework, VQ-SAM differs significantly in two aspects. First, *purpose-wise*, the approach of [8] focuses on refining the query and video features for VQL, while VQ-SAM aims at evolving the memory to extend SAM 2 for VQS. Second, *methodology-wise*, the method of [8] exploits only target cues for feature refinement, whereas our VQ-SAM leverages both target-specific information and background distractor cues for memory evolution, enabling more discriminative localization. In addition, a simple yet effective AMG module is specially designed for VQ-SAM to further improve the memory for better localization. To validate VQ-SAM, we conduct extensive experiments on VQS-4K. The results show that, our VQ-SAM demonstrates promising performance and largely surpasses current methods, establishing a solid foundation for future research on VQS.

In summary, we make the following contributions: ♠ We propose visual query segmentation (VQS), a new VQL paradigm segmenting *all pixel-level* target occurrences; ♥ We introduce VQS-4K, a large-scale dataset containing 4,111 videos for VQS; ♣ We present VQ-SAM, a simple yet effective approach to stimulate future research of VQS; ♦ We show VQ-SAM achieves promising results, expecting it to serve as a reference and provide guidance for future algorithm design.

2 Related Work

VQL Benchmark. Benchmark is crucial for training and evaluating VQL algorithms. To date, VQ2D, introduced as part of the Ego4D [9], is the only available

dataset tailored to this task. It contains 2,178 long first-person videos, which are divided into 5,842 clips under the current VQL paradigm, mainly focusing on locating the final target appearance using bounding boxes. ***Different from*** VQ2D, VQS-4K is specially developed for the new VQS task for more comprehensive and precise target localization. To this end, it provides pixel-level mask annotations for all target occurrences throughout the video (see Fig. 1 (b) again). Moreover, ***unlike*** VQ2D, which mainly focuses on locating rigid target objects from an egocentric viewpoint, VQS-4K aims at localizing arbitrary targets, rigid or deformable, across both first- and third-person views, which makes it more challenging yet practical in the real-world scenarios.

VQL Algorithm. VQL algorithms have recently witnessed rapid progress. The work of [31] proposes a two-stage VQL framework that first detects the target in a video and then performs bi-directional tracking from the detection result for spatial-temporal localization. To reduce compounding errors across different stages and to improve efficiency, the work of [11] introduces a single-stage end-to-end Transformer architecture for VQL, showing promising performance. Building on [11], the method of [8] applies a progressive framework to refine query and video features for more accurate localization, while the model in [2] explores attention guidance and egocentric augmentation to enhance performance. In [12], a simple yet effective training-free framework is presented to exploit foundational models for VQL, and shows excellent results. This approach is later extended in [13] with a better feature network. Unlike these methods, the work of [18] introduces an online VQL approach. ***Different from*** the above methods localizing the last target appearance with boxes as in existing VQL paradigm, VQ-SAM is specially developed for the new VQS task to segment all target occurrences at pixel-level, enabling more comprehensive and precise target localization.

Video object segmentation (VOS). VOS is a crucial vision task, aiming to separate foreground and background pixels in a video given the reference target. Owing to its key role in many applications, such as surveillance and autonomous vehicles, VOS has been extensively investigated in the past decade with many datasets (*e.g.*, [6, 10, 22, 23, 32, 34]) and methods (*e.g.*, [3, 4, 16, 19, 24, 25, 30, 33]) proposed. Similar to VOS, VQS segments the foreground target from background in a video. However, a key ***difference*** between them lies in the source of reference target. In VOS, the reference is directly obtained from the first frame *within* the search video, whereas in VQS, the reference target, or the visual query, is sampled from a frame *outside* the search video, making VQS more challenging. Besides, ***unlike*** VOS, which typically performs sequential *frame-level* propagation in a *trimmed* video, VQS requires *video-level* search from an *untrimmed* video, which increases the task complexity and necessitates different methodological designs.

3 The Proposed VQS-4K

3.1 Design Principle

We aim to provide a dedicated platform for visual query segmentation. In constructing the dataset, we adhere to the following key principles:

(1) *Dedicated benchmark.* One of the key motivations of this work is to provide a dedicated dataset for visual query segmentation. To align with the goal of VQS, each video sequence is paired with an external visual query, and annotated with spatial-temporal masklets corresponding to the query. Besides, to enable large-scale training and evaluation of models in current deep learning era, we expect the dataset to contain at least 4,000 videos.

(2) *Diverse object categories.* Diversity is crucial for a VQS dataset to support the development of generalizable VQS systems that are able to localize the target of arbitrary classes. To construct a diverse platform for VQS, we expect the new dataset to include at least 200 categories across diverse in-the-wild contexts.

(3) *High-quality annotation.* High-quality annotation is crucial for the dataset in both model training and evaluation. In order to ensure the high quality of our benchmark, each sequence is manually labeled with precise masklets for all target occurrences through iterative inspection and refinement.

3.2 Data Acquisition

Our dataset aims to facilitate the development of generalizable VQS by covering rich classes drawn from a wide range of real-world contexts. To this end, a diverse set of 222 object categories are selected in our VQS-4K. Following many existing video datasets (*e.g.*, [21,35]), the classes in VQS-4K are sourced from the popular ImageNet [5] and V3Det [29] datasets, and organized in a hierarchical structure. It is worth noting that, all selected categories in our VQS-4K are verified by the domain experts (*e.g.*, PhD students who work on related topics) to ensure their appropriateness for VQS. Compared to VQ2D, the classes in VQS-4K are more diverse and more desirable for visual query localization. Due to space limitation, we show the details of classes in VQS-4K in the **supplementary material**.

After determining the categories in VQS-4K, we then start searching for video sequences of each category from YouTube, the largest and the most popular video platform with massive real-world videos from various scenarios. Throughout the search process, only videos under the creative commons license are collected, and they are used exclusively for the research purpose. Initially, we collect more than 8K videos using keywords relevant to object classes. Then, we carefully inspect each video to verify its availability for VQS. Specifically, if a suitable pair that consists of a video clip and an external query outside the clip exists for our task, we keep it; otherwise, we discard it. After that, for each qualified video sequence, we select the identified pair of clip and query for our benchmark, and gather a total of 4,111 video-query pairs for VQS.

Eventually, we compile a large-scale dataset, termed VQS-4K, for visual query segmentation. VQS-4K contains 4,111 videos with 1.3 million frames and encompasses 222 categories from broad contexts. Each video is paired with an external visual query, and contains one or multiple target responses corresponding to the query. The average video length and the object response length are 52.9 and 9.4 seconds, respectively, at a frame rate of 6 frames per second (fps). Compared to VQ2D [9], which is the only benchmark for existing VQL paradigm, our VQS-4K offers more comprehensive and precise mask information as well as more diverse

Table 1: Summary of VQS-4K and its comparison with VQ2D that is used for current VQL paradigm and representative VOS datasets. “n/a” denotes that the statistic is not applicable to the dataset. LO: Last-Occurrence; AO: All-Occurrence; IV: Inside Video; OV: Outside Video. Please note that, the frame rates of all datasets are 6 *fps*.

Benchmark	Task	Videos	Object classes	Avg. vid. length	Avg. res. length	Total frames	Anno. frames	Mean occur.	Loc. aim	Refer. target	Object anno.
YT-VOS [32]	VOS	3,252	94	3.6 sec	n/a	0.11M	110K	n/a	n/a	IV	mask
LVOS [10]	VOS	220	27	95.4 sec	n/a	0.13M	130K	n/a	n/a	IV	mask
MOSE [6]	VOS	2,149	36	12.3 sec	n/a	0.16M	160K	n/a	n/a	IV	mask
VQ2D [9]	VQL	5,823	135	366.0 sec	2.7 sec	12.0M	266K	1	LO	OV	box
VQS-4K (ours)	VQS	4,111	222	52.9 sec	9.0 sec	1.3M	222K	2.9	AO	OV	mask

object categories for VQS. Tab. 1 summarizes our VQS-4K and its comparison to VQ2D [9] and representative related VOS datasets [6, 10, 32].

3.3 Data Annotation

In VQS-4K, each video is labeled with spatial-temporal masklets that correspond to the given external visual query, enabling precise localization and segmentation of the queried object across time. Specifically, for each pair of video and query, we first identify all temporal segments in the video in which the queried object appears. These segments may be non-contiguous and span multiple occurrences of the target throughout the video. Subsequently, within each identified temporal segment, we perform dense annotations on the target of interest indicated by the visual query at the frame level using temporally consistent spatial masks.

To ensure the high quality of annotations, we employ a multi-round, iterative labeling mechanism. Specifically, the experts first manually identify the start and the end timestamps of temporal segments for the queried target in each sequence. Then, the temporal segments of each video are manually labeled with masks by an annotation team formed by an expert and a few volunteers. After this initial round, the spatial-temporal mask annotations will be sent to a validation team of three experts for quality verification. If the annotations are not unanimously agreed by all experts, they will be returned back to the same labeling team for refinement. We repeat this process until annotations of all videos are completed. Due to limited space, we show the pipeline of our data annotation process in the **supplementary material**. Fig. 1 (b) displays several annotation examples in our VQS-4K, and more can be found in the **supplementary material**.

Statistics. To better understand our VQS-4K, we show representative statistics in Fig. 2, including the distributions of video length, response length, number of object occurrences, and object mask areas. From Fig. 2, we can observe that VQS-4K includes both long- and short-term videos, and individual videos often comprises multiple occurrences of the queried target. Together, these characteristics make the proposed VQS-4K well suited for real-world applications.

3.4 Dataset Split and Evaluation Metric

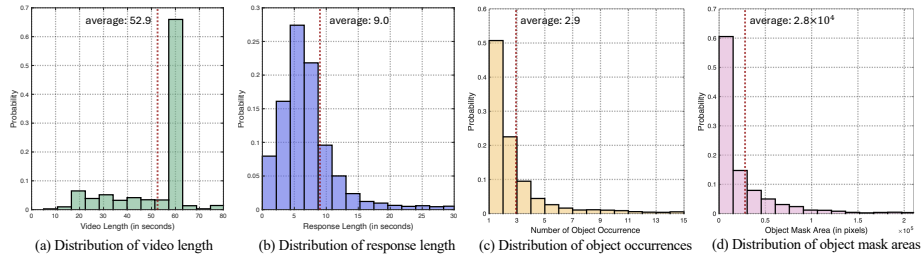


Fig. 2: Representative statistics on VQS-4K, including distributions of video length, response length, object occurrences, and object mask areas. Please note, values greater than 80 in video length are grouped into the final bin for visualization purposes.

Dataset Split. Our VQS-4K consists of a total of 4,111 videos. Among them, 3,289 videos with 1.04M frames are used for the training set (dubbed VQS-4K_{Tra}), and the rest 822 sequences with 264K frames are utilized for the testing set (dubbed VQS-4K_{Tst}). Both VQS-4K_{Tra} and VQS-4K_{Tst} contain the full

222 classes. In the dataset split, we try our best to make the distributions of these two sets close to each other. Tab. 2 shows the comparison of VQS-4K_{Tra} and VQS-4K_{Tst}, and the detailed splits will be released together with our data.

Besides, to enable further analysis, we divide VQS-4K_{Tst} into three subsets based on the average object mask area in each video, including VQS-4K_{Tst}-Small for *small-scale* objects with average mask areas in the range of $[0, 3.6 \times 10^3]$ pixels (269 videos), VQS-4K_{Tst}-Medium for *medium-scale* objects with average mask areas in $[3.6 \times 10^3, 4.0 \times 10^4]$ pixels (393 videos), and VQS-4K_{Tst}-Large for *large-scale* objects with average mask areas greater than 4.0×10^4 pixels (164 videos).

Evaluation Metric. We employ multiple metrics on our VQS-4K for evaluation, comprising *spatial-temporal Average Precision* (stAP), stAP₅₀, stAP₇₅, *temporal Average Precision* (tAP), tAP₅₀, tAP₇₅, *Recovery* (Rec), and *Success* (Succ). More specifically, stAP measures the accuracy of spatio-temporal prediction, and is computed as the average mask IoU between predicted spatial-temporal masks and groundtruth, and stAP₅₀ and stAP₇₅ respectively apply IoU thresholds of 0.5 and 0.75, where only predictions whose mask IoU is greater the corresponding threshold are counted as correct. Different from stAP, tAP is applied to evaluate the accuracy of temporal prediction, and calculated as the average temporal IoU between the predicted temporal occurrences and the groundtruth, and similarly, tAP₅₀ and tAP₇₅ employ the IoU thresholds of 0.5 and 0.75. Similar to [9], the recovery is to evaluate the percentage of predicted frames in which the mask IoU between mask prediction and groundtruth exceeds 0.5, and the success measures whether the mask IoU between prediction and groundtruth is above 0.2. Please note, we adopt a stricter success threshold of 0.2, instead of 0.05 as in [9], since videos in our dataset are much shorter and contain more object occurrences.

Table 2: Comparison between the training and the testing sets of VQS-4K.

	Videos	Avg. Vid. length	Avg. res. length	Total frames	Mean occur.
VQS-4K _{Tst}	822	53.3 sec	6.9 sec	264K	2.7
VQS-4K _{Tra}	3,289	52.8 sec	9.5 sec	1.04M	3.0

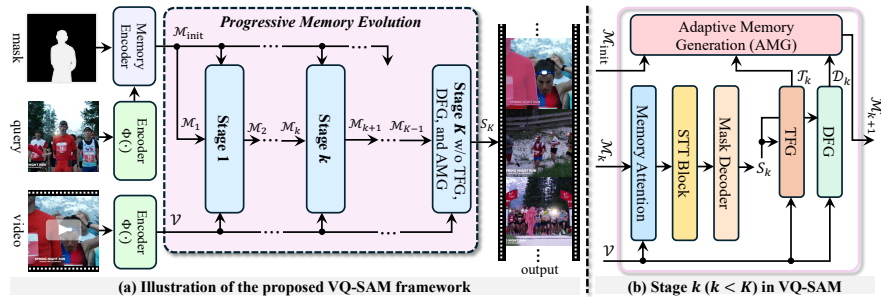


Fig. 3: Overview of VQ-SAM that mines target and background distractor information in the video via a progressive framework for VQS. Please *note* that, the last stage K outputs S_K for the final prediction, and TFG, DFG, and AMG modules are removed.

4 Methodology: A New Baseline for VQS

Formulation. VQS is formulated as a spatio-temporal segmentation task in the open-set environment. Specifically, given an untrimmed video and a visual query with a mask indicating the object of interest, the goal is to segment *all pixel-level* target occurrences. The results is a spatial-temporal mask response $\mathcal{R} = \{R_i\}_{i=1}^P$ containing one or multiple masklets of object occurrences, where P denotes the number of object occurrences and each $R_i = \{r_i^s, \dots, r_i^e\}$ represents the i^{th} object occurrence with e and s its start and end frame indices and r_i^j the mask indicating the target in frame j . Examples of R can be seen in Fig. 1 (b).

Overview. We propose VQ-SAM for VQS by extending SAM 2 [25]. The core is to exploit target and distractor cues via a multi-stage framework to progressively evolve the memory for VQS (Sec. 4.1). As in Fig. 3, at each stage, except for the final prediction stage, VQ-SAM mines confident target and distractor features using current memory. These features, together with the initial memory from visual query, are sent to AMG (Sec. 4.2) to generate new memory for the next stage, enabling more accurate target and distractor features for further memory evolution. Through this progressive process, the memory in VQ-SAM is gradually improved, leading to better localization and segmentation in the final stage.

4.1 The VQ-SAM Framework

Feature Extraction. In VQ-SAM, we first extract features for the visual query and video frames. Specifically, given the visual query Q and L frames $\mathcal{I} = \{I_i\}_{i=1}^L$ from the video, we use a shared encoder $\Phi(\cdot)$ to extract their features $f_Q = \Phi(Q)$ and $\mathcal{V} = \{f_i\}_{i=1}^L$ with each $f_i = \Phi(I_i)$. Afterwards, the feature f_Q of the visual query, together with its given target mask m_Q , are applied to generate the initial memory $\mathcal{M}_{\text{init}} = \text{MemEnc}(f_Q, m_Q)$, where $\text{MemEnc}(\cdot, \cdot)$ is the memory encoder from SAM 2 [25]. After feature extraction, we propose a multi-stage framework to progressively evolve the memory by exploring target and distractor cues.

Progressive Memory Evolution for VQS. Due to severe target appearance changes and the presence of similar distractors in the video, relying solely on the

initial memory, generated by the visual query, is *insufficient* for localization and segmentation. Addressing this, VQ-SAM explores target-specific and background distractor features in the video to progressively evolve the memory for VQS with a multi-stage framework. In each but the last stage, we mine the confident target and background distractor features using current memory, which, together with the initial memory, are used to generate a new memory for the next stage.

Specifically, for the k^{th} ($1 \leq k < K$) stage of VQ-SAM, let M_k be the current memory. In the first stage ($k = 1$), $\mathcal{M}_1 = \mathcal{M}_{\text{init}}$, initialized with $\mathcal{M}_{\text{init}}$. To mine target and distractor features in a video, we first generate the mask candidates in each frame using \mathcal{M}_k , and then select target and distractor masks from them to extract features. Concretely, we first fuse current memory \mathcal{M}_k into the video features using memory attention via

$$\tilde{\mathcal{V}}_k = \{\tilde{f}_i^k\}_{i=1}^L \quad \tilde{f}_i^k = \text{MemAtt}(f_i, \mathcal{M}_k) \quad (1)$$

where $\tilde{\mathcal{V}}_k$ denotes the video features after fusion, and $\text{MemAtt}(\cdot, \cdot)$ is the memory attention [25]. To capture video temporal context, we employ a spatial-temporal Transformer (STT) block to enhance video features before mask decoding via

$$\hat{\mathcal{V}}_k = \text{STTB}(\tilde{\mathcal{V}}_k) \quad (2)$$

where $\hat{\mathcal{V}}_k = \{\hat{f}_i^k\}_{i=1}^L$ denotes the enhanced video features with \hat{f}_i^k the feature of frame i . $\text{STTB}(\cdot)$ is the SST block, composed of feature flattening, self-attention layers [27], and feature reshaping, as detailed in the **supplementary material**. After this, we apply mask decoder $\text{MaskDec}(\cdot)$ in [25] on each \hat{f}_i^k to obtain mask candidates in frame i , as follows,

$$M_i^k = \text{MaskDec}(\hat{f}_i^k) \quad (3)$$

where $M_i^k = \{m_{i,h}^k\}_{h=1}^H$ denotes the set of mask candidates, and H the number of candidates (H is set to 3 as in [25]). In M_i^k , each predicted $m_{i,h}^k$ contains the mask token, a predicted IoU score, and an occlusion score.

Once obtaining mask candidates $S_k = \{M_i^k\}_{i=1}^L$ in the video, we employ two modules, *i.e.*, target feature generation (TFG) and distractor feature generation (DFG) as explained later, to select the target-specific and distractor masks and extract their features, as follows,

$$\mathcal{T}_k = \text{TFG}(\mathcal{V}, S_k) \quad \mathcal{D}_k = \text{DFG}(\mathcal{V}, S_k) \quad (4)$$

where \mathcal{T}_k and \mathcal{D}_k represent the features of selected n_t target and n_d distractor masks, which, together the initial memory $\mathcal{M}_{\text{init}}$ from query, are fed to our AMG (Sec 4.2) to generate the new memory, as follows,

$$\mathcal{M}_{k+1} = \text{AMG}(\mathcal{M}_{\text{init}}, \mathcal{T}_k, \mathcal{D}_k) \quad (5)$$

where \mathcal{M}_{k+1} is the new memory, which is sent to the next stage ($k+1$) to generate more accurate target and distractor features for further memory evolution.

In the final K^{th} stage, we perform localization and segmentation, and TFG, DFG, and AMG modules are removed. Given \mathcal{M}_K and video features \mathcal{V} , we first generate the mask candidates $S_K = \{M_i^K\}_{i=1}^L$ via Eqs. (1)-(3), and then identify the mask with the highest IoU score in each frame i . This mask is selected as the final prediction in frame i if its corresponding occlusion score is above 0; otherwise, the prediction is set to empty *i.e.*, target does not exist.

Target Feature Generation (TFG). TFG aims to select target masks from a video and extract their features. Given $S_k = \{M_i^k\}_{i=1}^L$, we first identify mask $b_i^k \in M_i^k$ which has the highest IoU score in each frame i . To ensure mask quality, we remove those b_i^k whose IoU scores are below a threshold τ_t . After this, from the remaining masks, we select the top n_t ones ranked by IoU score, which are then encoded using the memory encoder in [25] to obtain the target features \mathcal{T}_k . Since \mathcal{T}_k is derived from reliable target-specific masks in the video, it can be used to improve memory in handling target appearance changes.

Distractor Feature Generation (DFG). Unlike TFG, DFG selects a few top distractor masks and extract their features. Similar to [28], the distractor masks are selected from alternative mask candidates, *i.e.*, all candidates except the best one in each frame. We first identify the best mask $b_i^k \in M_i^k$ in frame i with the highest IoU score. Then, for each alternative mask x , we compute its divergence score with respect to b_i^k via $1 - \text{IoU}(b_i^k, x)$, where $\text{IoU}()$ is to calculate the mask IoU, to measure spatial discrepancy between the best mask and the alternative candidate. To ensure diversity from the target and discriminative difficulty, we only keep alternative masks whose divergence and predicted IoU scores exceed pre-defined thresholds τ_d and τ_s . From all qualified alternative masks in the video, we select the top n_d masks ranked by the product of divergence and IoU scores, and extract their features as in [28] to obtain the distractor features \mathcal{D}_k . If there are no qualified alternative masks, \mathcal{D}_k is empty and ignored in generating new memory. By incorporating \mathcal{D}_k into memory, VQ-SAM is able to resist to distinguish target from background distractors in localization.

4.2 Adaptive Memory Generation (AMG)

Considering different features, including $\mathcal{M}_{\text{init}}$, \mathcal{T}_k , and \mathcal{D}_k , may contribute unequally in the new memory, we design a simple yet effective adaptive memory generation (AMG) module that dynamically learns their relative importance and integrates them accordingly. Specifically, we first apply global pooling to \mathcal{T}_k and \mathcal{D}_k , respectively, to fuse target and distractor features, followed by an MLP for dimensionality reduction, as follows,

$$\tilde{\mathcal{T}}_k = \text{MLP}(\text{GP}(\mathcal{T}_k)) \quad \tilde{\mathcal{D}}_k = \text{MLP}(\text{GP}(\mathcal{D}_k)) \quad (6)$$

Then, we concatenate $\mathcal{M}_{\text{init}}$, $\tilde{\mathcal{T}}_k$, and $\tilde{\mathcal{D}}_k$, and feed them into an MLP followed by softmax normalization to learn adaptive importance weights, as follows,

$$w = \text{Softmax}(\text{MLP}(\text{Concat}(\mathcal{M}_{\text{init}}, \tilde{\mathcal{T}}_k, \tilde{\mathcal{D}}_k))) \quad (7)$$

where $w = [w_1, w_2, w_3] \in \mathbb{R}^{1 \times 3}$ represents the learned weights for $\mathcal{M}_{\text{init}}$, \mathcal{T}_k , and \mathcal{D}_k , respectively. Afterwards, we generate the new memory \mathcal{M}_{k+1} , as follows,

$$\mathcal{M}_{k+1} = \{w_1 \cdot \mathcal{M}_{\text{init}}, w_2 \cdot \mathcal{T}_k, w_3 \cdot \mathcal{D}_k\} \quad (8)$$

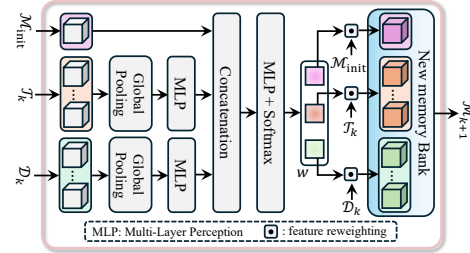


Fig. 4: Architecture of our AMG.

Fig. 4 displays the architecture of AMG. Please note that, when \mathcal{D}_k is empty due to no distractors, we only learn the weights $w = [w_1, w_2] \in \mathbb{R}^{1 \times 2}$ for $\mathcal{M}_{\text{init}}$ and \mathcal{T}_k . Compared with memory generation using fixed or uniform weights, AMG adaptively modulates the contribution of different feature sources, enabling more context-aware and discriminative memory generation.

4.3 Optimization and Inference

Optimization. Given the video and the visual query with an object mask, VQ-SAM predicts mask candidates $S_k = \{M_i^k\}_{i=1}^L$ for each stage k . During training, given the groundtruth, following SAM 2 [25], we utilize multiple losses, including dice coefficient loss, penalties residual activation loss, IoU loss, and binary cross-entropy loss for the loss function \mathcal{L}_k^i in the i^{th} frame (please see [25] for details). Then, the loss \mathcal{L}_k in stage k is calculated as $\mathcal{L}_k = \sum_{i=1}^L \mathcal{L}_k^i$, and the total training loss $\mathcal{L}_{\text{total}} = \sum_{k=1}^K \gamma_k \mathcal{L}_k$ with γ_k the loss weight for stage k .

Inference. In inference, with $S_K = \{M_i^K\}_{i=1}^L$ from the final stage K , we identify the mask with the highest IoU score in each frame. If its occlusion is above zero, this mask is selected as the prediction in this frame. Otherwise, the prediction is set to empty. Please note that, due to the memory constraint, we divide a video into small clips and perform inference on each of the clip, and the final response is obtain by merging the inference result from each clip.

5 Experiments

Implementation. Our VQ-SAM is implemented using PyTorch [20] on a machine with 4 Nvidia A6000 GPUs. Similar to [25], the encoder $\Phi(\cdot)$ adopts Hierar-B+ [26] with feature pyramid network (FPN) [15] for feature extraction. We train VQ-SAM for 144 epoches with a batch size of 4 using AdamW [17] with an initial learning of 5×10^{-6} . During training and inference, the query image and video frames are resized to 768×768 . The video length L is set to 7 due to memory constraints. The number of stages K is empirically set to 2. The thresholds τ_t , τ_d , and τ_s are set to 0.5, 0.5, and 0.7. The numbers of selected target and distractor masks n_t and n_d in TFG and DFG are set to 2 and 1, respectively. The loss weights γ_1 and γ_2 are empirically set to 0.5 and 1.0.

5.1 State-of-the-art Comparison

Since there are no available approaches specifically designed for VQS, we adapt video object segmentation (VOS) models [1, 3, 7, 14, 24, 25, 28] and visual query localization (VQL) approaches [8, 11, 13] for comparison. For VOS methods, the target reference is the visual query with object mask. For VQL models, we add an additional prediction head with convolutional and upsampling layers to output masks (see the architecture in **supplementary material**). For consistency with VQS, VQL methods are designed to output all target masks. For fair comparison, all these models, except for the train-free method [13], are trained on VQS-4K_{Tra}.

Table 3: Comparison with current approaches on VQS-4K_{Tst}.

Methods	stAP	stAP ₅₀	stAP ₇₅	tAP	tAP ₅₀	tAP ₇₅	Rec	Succ
Cutie-b[CVPR'24] [3]	18.5	16.5	8.2	21.0	16.9	9.2	38.4	32.3
OASIS[ICCV'25] [24]	15.8	13.6	6.7	21.3	17.4	9.5	34.3	29.4
LOMM[ICCV'25] [14]	12.5	10.2	5.0	12.7	7.9	4.3	26.1	25.8
SAM 2[ICLR'25] [25]	12.9	10.6	5.2	13.0	8.3	4.6	26.7	26.3
SAM2.1++[CVPR'25] [28]	12.5	10.2	5.1	14.6	10.0	5.5	28.8	25.8
SAM2Long[ICCV'25] [7]	18.6	16.5	8.2	24.4	20.6	11.2	38.6	32.5
SAM 3[ICLR'26] [1]	13.3	10.9	5.4	14.1	9.5	5.2	27.7	26.6
VQLoC[NeurIPS'23] [11]	10.1	12.5	6.3	21.5	17.5	8.4	31.7	23.2
PRVQL[ICCV'25] [8]	13.6	14.4	7.1	22.1	18.4	8.7	32.6	26.9
REN[NeurIPS'25] [13]	16.8	17.7	8.9	23.6	19.8	9.5	34.8	30.5
VQ-SAM (ours)	26.0	23.8	12.7	29.6	26.8	14.4	43.6	42.1

Table 4: Comparison of different methods on VQS-4K_{Tst}-Small, VQS-4K_{Tst}-Medium, and VQS-4K_{Tst}-Large. Our VA-SAM consistently achieves the best performance.

Methods	VQS-4K _{Tst} -Small				VQS-4K _{Tst} -Medium				VQS-4K _{Tst} -Large			
	stAP	tAP	Rec	Succ	stAP	tAP	Rec	Succ	stAP	tAP	Rec	Succ
Cutie-b[CVPR'24] [3]	13.3	17.2	29.9	25.5	19.0	21.4	39.6	33.8	25.6	26.1	45.4	39.8
OASIS[ICCV'25] [24]	11.4	17.4	26.7	23.2	16.2	21.7	35.4	30.7	21.9	26.5	40.5	36.2
LOMM[ICCV'25] [14]	9.0	10.4	20.4	20.3	12.8	13.0	26.9	27.0	17.3	15.8	30.8	31.8
SAM 2[ICLR'25] [25]	9.3	10.6	20.8	20.7	13.2	13.3	27.6	27.5	17.9	16.2	31.6	32.4
SAM2.1++[CVPR'25] [28]	9.1	11.9	22.5	20.3	12.8	14.9	29.7	27.0	17.3	18.1	34.0	31.8
SAM2Long[ICCV'25] [7]	13.4	19.9	30.1	25.6	19.1	24.9	39.9	34.0	25.8	30.4	45.6	40.0
SAM 3[ICLR'26] [1]	9.6	11.5	21.5	21.0	13.6	14.4	28.6	27.8	18.4	17.5	32.7	32.7
VQLoC[NeurIPS'23] [11]	7.3	17.6	24.7	18.3	10.4	21.9	32.7	24.3	14.0	26.7	37.5	28.6
PRVQL[ICCV'25] [8]	9.8	18.1	25.4	21.2	14.0	22.5	33.7	28.1	18.9	27.5	38.5	33.1
REN[NeurIPS'25] [13]	12.1	19.3	27.1	24.0	17.2	24.1	35.9	31.9	23.3	29.4	41.2	37.5
VQ-SAM (ours)	18.8	24.3	34.0	33.2	26.7	30.2	45.0	44.0	36.0	36.8	51.5	51.8

Tab. 3 reports the results. We can observe that, our VQ-SAM outperforms all other approaches by a large margin on all metrics. Specifically, VQ-SAM achieves the best stAP score with 26.0% and tAP score with 26.8%, which surpasses the second best SAM2Long with 18.6% stAP and 24.4% tAP by 7.4% and 5.2%, clearly showing its superiority. Compared with the state-of-the-art VQL method REN with 16.8% stAP and 23.6% tAP, our VQ-SAM outperforms it by 9.2% in stAP and 6.0% in tAP, evidencing the strength of our method. Compared to SAM 2, which can be seen as our baseline, VQ-SAM obtains gains of 13.1% and 16.6% in stAP and tAP, showing the importance of modeling temporal context and exploring target and distractor cues for VQS. Moreover, from Tab. 3, we observe that several recent VOS methods such as OASIS, LOMM, SAM2.1++, and SAM 3 struggle in VQS. This highlights the unique challenges posed by VQS, particularly in conducting video-level search within untrimmed videos.

In addition, we compare different approaches across different scales on three subsets of VQS-4K, comprising 4K_{Tst}-Small for small-scale objects, VQS-4K_{Tst}-Medium for medium-scale objects, and VQS-4K_{Tst}-Large for large-scale objects, using stAP, tAP, Rec, and Succ. The results are shown in Tab. 4. From Tab. 4, we can observe that, our VQ-SAM consistently shows the best performance for objects with different scales over all metrics, showing its robustness.

Table 5: Ablation on TFG and DFG.

	TFG	DFG	stAP	tAP	Rec	Succ
❶			23.8	24.9	36.7	27.1
❷	✓		24.8	25.4	38.3	31.8
❸		✓	25.4	27.3	41.1	37.0
❹	✓	✓	26.0	29.6	43.6	42.1

Table 6: Ablation on the STT block.

		stAP	tAP	Rec	Succ
❶	w/o STT block	25.2	27.9	39.7	36.1
❷	w/ STT block	26.0	29.6	43.6	42.1

Table 9: Ablation on n_t in TFG.

		stAP	tAP	Rec	Succ
❶	$n_t = 1$	25.0	28.6	42.0	39.8
❷	$n_t = 2$	26.0	29.6	43.6	42.1
❸	$n_t = 3$	25.1	28.6	42.1	40.0

Table 7: Ablation on number of stages.

		stAP	tAP	Rec	Succ
❶	$K = 1$	21.5	13.9	17.3	8.2
❷	$K = 2$	26.0	29.6	43.6	42.1
❸	$K = 3$	25.1	28.6	44.8	39.8

Table 8: Ablation on memory generation.

		stAP	tAP	Rec	Succ
❶	EMG	23.9	27.0	41.2	38.4
❷	SLMG	25.1	28.7	42.4	39.7
❸	AMG	26.0	29.6	43.6	42.1

Table 10: Ablation on n_d in DFG.

		stAP	tAP	Rec	Succ
❶	$n_d = 1$	26.0	29.6	43.6	42.1
❷	$n_d = 2$	24.2	28.0	41.3	38.3
❸	$n_d = 3$	23.7	26.6	39.2	37.0

5.2 Ablation Studies

To better understand VQ-SAM, we conduct ablation studies on VQS-4K_{Tst} using stAP, tAP, Rec%, and Succ, with our final configuration highlighted in cyan.

Impact of TFG and DFG. In VQ-SAM, TFG and DFG are employed to mine target and distractor cues in the video for memory evolution. To analyze their impacts, we conduct ablation studies in Tab. 5. We can see that, without TFG and DFG, the stAP and tAP scores are 23.8% and 24.9% (❶). When applying TFG along, stAP and tAP are improved to 24.8% and 25.4% with 1.0% and 0.5% gains (❷ *v.s.* ❶), showing that target information from the video benefits the target localization and segmentation. When use DFG along, stAP and tAP are improved to 25.4% and 27.3% with 1.6% and 2.4% gains (❸ *v.s.* ❶), indicating the importance of exploring distractor cues for VQS. When using both TFG and DFG, we achieve the best performance with 26.0% stAP and 29.6% tAP (❹ *v.s.* ❶), evidencing the efficacy of our memory evolution for improving VQS.

Impact of the STT block. To capture global temporal context in the video for VQS, we apply a spatial-temporal Transformer block in each stage of VQ-SAM. To investigate its impact, we conduct the ablation studies in Tab. 6. From Tab. 6, we observe that, without STT, the stAP and tAP scores are 25.2% and 27.9% (❶). When applying STT in VQ-SAM, stAP and tAP scores are improved to 26.0% and 29.6% (❷), evidencing the effectiveness of STT for improving VQS.

Impact of the number of stages. VQ-SAM is a progressive framework with K stages to evolve the memory using target and distractor information. We conduct ablation studies on K in Tab. 7. We observe that, when setting $K = 1$, which means no target and distractor information is explored for memory evolution, the stAP and tAP are 21.5% and 13.9% (❶). When adding a stage, the stAP and tAP are significantly improved to 26.0% and 29.6% (❷), showing the importance of target and distractor cues for VQS. When further increasing the stage number to 3 (❸), the performance is slightly decreased. Thus, we set K to 2 in this work.

Impact of AMG. In VQ-SAM, we propose adaptive memory generation (AMG) to integrate different features for memory generation. To study its effectiveness, we conduct an ablation study by comparing AMG with two alternative strategies, including equal-weight memory generation (EMG) and static learnable memory generation (SLMG). EMG integrates different features using fixed equal weights, whereas SLMG assigns globally learnable weights to each feature type, which are fixed after training (see the architecture of SLMG in the **supplementary material**). In contrast, AMG dynamically predicts weights conditioned on current features, enabling adaptive memory construction. From Tab. 8, we can see that, using AMG achieves the best results (③ *v.s* ①/②), showing its efficacy.

Impact of n_t in TFG. In VQ-SAM, n_t controls the number of selected target masks for the new memory generation. We conduct an ablation on n_t in Tab. 9. When selecting two target masks, we achieve the best performance (②). When increasing n_t to 3, the performance slightly drops (③), which may be caused by the noise in the additional features. Thus, we set n_t to 2 in our method.

Impact of n_d in DFG. n_d determines the number of selected distractor masks for memory evolution. As shown in the ablation in Tab. 10, when using only one distractor for memory evolution, VQ-SAM shows best results (①).

5.3 Comparison with Existing VQL Methods on VQ2D

Although VQ-SAM is designed for the proposed VQS task, it can also be used for VQL. To validate this, we conduct an experiment on VQ2D [9] and compare it with representative VQL methods. Please note that for VQL evaluation, the mask outputs of VQ-SAM are converted into bounding boxes to ensure consistency with VQL (please see more details in the **supplementary material**). Tab. 11 reports the results. From Tab. 11, we can observe that, even VQ-SAM is not specifically design for VQL, it still achieves the best performance on all metrics, validating its efficacy.

Due to limited space, please refer to our **supplementary material** for more results and details, additional analysis, and ablation studies.

Table 11: Comparison with existing VQL methods on the VQ2D validation set [9].

Methods	stAP	tAP	Rec	Succ
VQLoC _[ICCV'25] [11]	23.7	32.3	45.1	55.9
PRVQL _[ICCV'25] [8]	28.1	36.8	45.7	59.4
RELOCATE _[CVPR'25] [12]	35.2	42.9	50.6	60.1
RENDINOv2 _[NeurIPS'25] [13]	39.7	51.6	49.3	61.2
VQ-SAM (ours)	41.8	56.0	53.8	64.2

6 Conclusion

In this work, we propose VQS, a new paradigm of VQL aiming at segmenting all pixel-level occurrences of an object of interest from an untrimmed video, enabling more comprehensive and precise localization. To facilitate the research on VQS, we introduce a large-scale benchmark VQS-4K by including 4,111 videos with more than 1.3 million frames. Moreover, to stimulate future research, we present VQ-SAM, a simple but effective method for VQS. Our experiments on VQS-4K validates the effectiveness of VQ-SAM. Through VQS-4K and VQ-SAM, we hope to inspire more research as well as practical applications on VQS.

Supplementary Material

To better understand this work, we offer additional details, analysis, and results as follows:

- **S1 Details of Object Categories**
In this section, we provide the details of object classes in VQS-4K.
- **S2 Construction Pipeline of VQS-4K and Additional Annotation Examples**
In this section, we describe the detailed construction pipeline of our VQS-4K, and provide more annotation examples.
- **S3 More Statistics**
This section shows more statistics on our benchmark,
- **S4 Details of Evaluation Metrics**
In this section, we provide the detailed calculation of the adopted evaluation metrics.
- **S5 Additional Results and Analysis**
In this section, we provide additional results and analysis of our work.
- **S6 Ethical Statement and Maintenance of VQS-4K**
This section discusses the ethical statement and maintenance of VQS-4K.

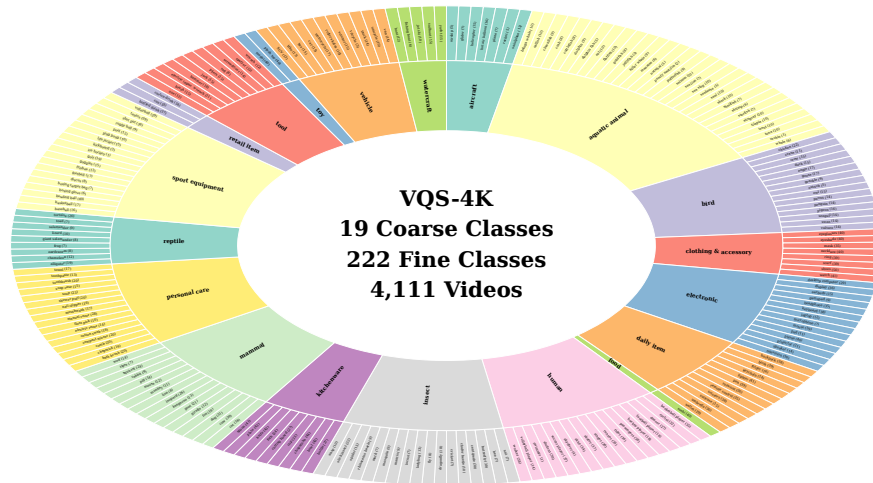


Fig. 5: Category organization of VQS-4K. The inner part of chart displays 19 coarser classes, while the outer part shows 222 fine categories. Best viewed by zooming in.

S1 Details of Object Categories

VQS-4K comprises 222 object classes, aiming to offer a diverse platform for VQS. These categories are organized in the hierarchical structure. Specifically, we first

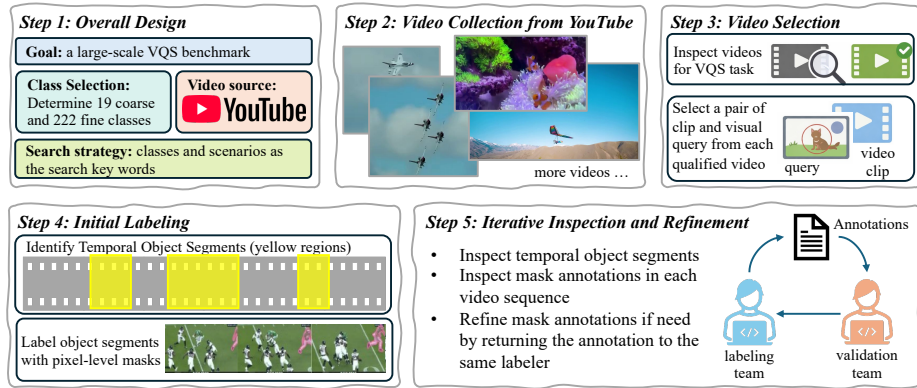


Fig. 6: Construction pipeline of VQS-4K, including five steps, *i.e.*, overall design, video collection, video selection, initial labeling, and iterative inspection and refinement.

determine 19 coarse object classes, including “human”, “insect”, “kitchenware”, “mammal”, “personal care”, “reptile”, “sport equipment”, “retail item”, “tool”, “toy”, “vehicle”, “watercraft”, “aircraft”, “aquatic animal”, “bird”, “clothing & accessory”, “electronic”, “daily item”, and “food”. Please note that, since “human” is a special category, we separate it from “mammal”. After this, we further gather 222 fine categories from 19 coarse classes. Fig. 5 shows the category organization of VQS-4K (please zoom in for best view).

S2 Construction Pipeline of VQS-4K and Additional Annotation Examples

In this paper, we adopt a systematic five-step pipeline to construct VQS-4K: (i) **Overall design**. In the first step, we determine all object categories in VQS-4K and a video search strategy using class names and scenarios as keywords. (ii) **Video collection**. The second step is to collect video sequences from YouTube using the strategy in the first step. Please note, all videos in VQS-4K are collected under the *creative commons* license and used for *research purpose only*. (iii) **Video selection**. The third step is to inspect videos collect in the second step to verify their availabilities for VQS. We will select a pair of clip and visual query from each qualified video. (iv) **Initial labeling**. The fourth step is to conduct initial labeling by experts. Specifically, for each pair of video and query, we first identify all temporal segments in the video in which the queried object appears. Then, within each identified temporal segment, pixel-level masks will be provided for the target of interest. (v) **Iterative inspection and refinement**. In the final step, multiple rounds of iterative inspection and refinement if needed are performed by experts and volunteers to ensure high annotation quality. Fig. 6 shows the construction pipeline. In Fig. 7, we provide more annotation examples in the proposed VQS-4K.

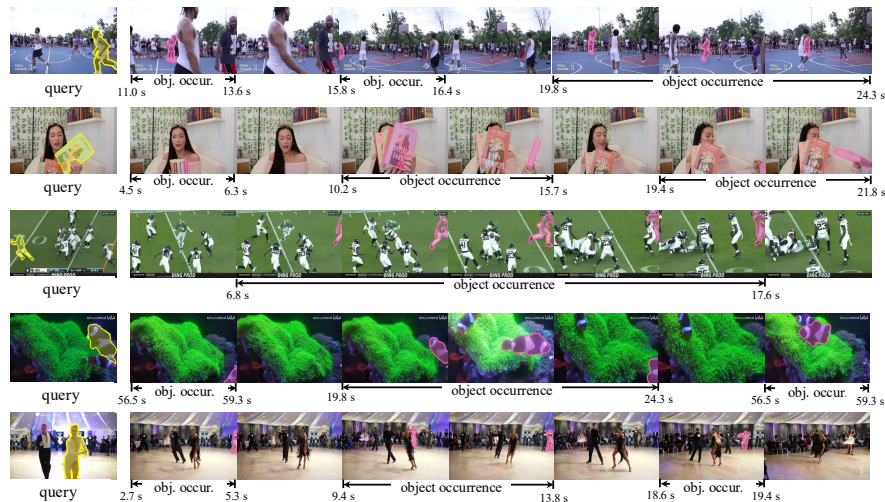


Fig. 7: Additional annotation samples in the proposed VQS-4K.

S3 More Statistics

In order to better understand our VQS-4K, we further demonstrate other representative statistics. Specifically, we show the distributions of relative area to the initial target and Intersection over Union (IoU) between the targets in adjacent frames with in temporal object segments in Fig. 8. These two statistics can reflect the motion information of the target in the video. From Fig. 8, we can observe that that queried target moves fast and varies in scale rapidly in the videos.

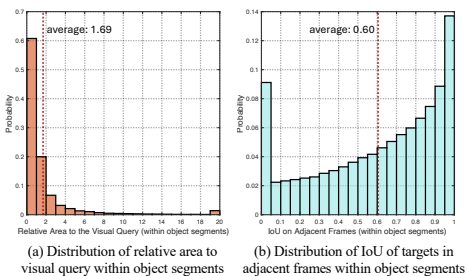


Fig. 8: More statistics.

S4 Details of Evaluation Metrics

We adopt multiple metrics to comprehensively evaluate both temporal and spatial-temporal localization performance for VQS. We report $stAP$, $stAP_{50}$, $stAP_{75}$, tAP , tAP_{50} , tAP_{75} , Recovery (Rec), and Success (Succ). Specifically, $stAP$ and tAP measure localization accuracy by averaging per-video overlap scores over the testing set $VQS-4K_{Tst}$, and are calculated as follows,

$$stAP = \frac{1}{|\mathbf{V}_{tst}|} \sum_{v \in \mathbf{V}_{tst}} stIoU_v \quad tAP = \frac{1}{|\mathbf{V}_{tst}|} \sum_{v \in \mathbf{V}_{tst}} tIoU_v \quad (9)$$

where \mathbf{V}_{tst} denotes the set of videos in the $VQS-4K_{Tst}$, and $|\mathbf{V}_{tst}|$ is the number of videos in \mathbf{V}_{tst} . $stIoU_v$ and $tIoU_v$ are $stIoU$ (*i.e.*, overlap between groundtruth and

predicted masks across all frames) and tIoU (*i.e.*, overlap between groundtruth and predicted temporal segments) scores in video v , and computed as follows,

$$\text{stIoU}_v = \frac{\sum_{t \in v_{\text{gt}} \cup v_{\text{pred}}} |\mathcal{R}_t^{\text{gt}} \cap \mathcal{R}_t^{\text{pred}}|}{\sum_{t \in v_{\text{gt}}} |\mathcal{R}_t^{\text{gt}}| + \sum_{t \in v_{\text{pred}}} |\mathcal{R}_t^{\text{pred}}| - \sum_{t \in v_{\text{gt}} \cup v_{\text{pred}}} |\mathcal{R}_t^{\text{gt}} \cap \mathcal{R}_t^{\text{pred}}|} \quad (10)$$

$$\text{tIoU}_v = \frac{|\mathcal{F}_{v_{\text{gt}}} \cap \mathcal{F}_{v_{\text{pred}}}|}{|\mathcal{F}_{v_{\text{gt}}} \cup \mathcal{F}_{v_{\text{pred}}}|} \quad (11)$$

where $\mathcal{R}_t^{\text{gt}}$ and $\mathcal{R}_t^{\text{pred}}$ are groundtruth and predicted masks at frame t in video v . $\mathcal{F}_{v_{\text{gt}}}$ and $\mathcal{F}_{v_{\text{pred}}}$ are the sets of frames containing the groundtruth and predicted masks in video v . With stAP and tAP, stAP_τ and tAP_τ are computed as follows,

$$\text{stAP}_\tau = \frac{1}{|\mathbf{V}_{\text{tst}}|} \sum_{v \in \mathbf{V}_{\text{tst}}} \mathbb{I}[\text{stIoU}_v \geq \tau] \cdot \text{stIoU}_v \quad (12)$$

$$\text{tAP}_\tau = \frac{1}{|\mathbf{V}_{\text{tst}}|} \sum_{v \in \mathbf{V}_{\text{tst}}} \mathbb{I}[\text{tIoU}_v \geq \tau] \cdot \text{tIoU}_v \quad (13)$$

where $\tau \in \{0.5, 0.75\}$ is the threshold. $\mathbb{I}[\cdot]$ is the indicator function that return 1 if the condition is true and 0 otherwise.

Different from stAP and tAP, the recovery is to evaluate the percentage of predicted frames in which the mask IoU between mask prediction and groundtruth exceeds 0.5, and the success measures whether the mask IoU between prediction and groundtruth is above 0.2.

S5 Additional Results and Analysis

S5.1 Impact of γ_k in Optimization

In VQ-SAM, multiple stages are jointly optimized, and the loss of each stage is controlled by a corresponding weight γ_k (see Sec. 4.3). To study the impact of γ_k (*i.e.*, γ_1 and γ_2 for the two stages in VQ-SAM), we conduct an ablation study in Tab. 12. From Tab. 12, we can see that, when setting γ_1 and γ_2 to 0.5 and 1.0, respectively, we achieve the best results on all metrics (see ②).

Table 12: Ablation study on γ_1 and γ_2 .

	γ_1	γ_2	stAP	tAP	Rec	Succ
①	0.5	0.5	24.2	27.0	40.4	39.0
②	0.5	1.0	26.0	29.6	43.6	42.1
③	1.0	0.5	24.5	27.4	41.2	39.9
④	1.0	1.0	25.3	28.7	42.2	40.8

S5.2 Memory Requirement and Model Efficiency of VQ-SAM

We train VQ-SAM using 4 Nvidia A6000 (48G) GPUs for around 62 hours. The resolution of videos for both training and testing is 768×768 . In inference, the GPU memory requirement for running VQ-SAM is 9.7G for an eight-frame video clip, and the inference speed on Nvidia A6000 GPU is 29 frames per second (fps).

S5.3 Annotation Accuracy Analysis.

To analyze annotation accuracy, we randomly select 150 videos in VQS-4K and ask an independent group for re-labeling. After this, we compute the Intersection over Union (IoU) of the new and original annotations, and the IoU is 0.92, showing the reliability of our annotations.

S5.4 Visualization of Selected Target and Distractor Cues

VQ-SAM aims to mine target and distractor cues from the video for evolving the memory for better visual query segmentation. In Fig. 9, we show the selected target and distractor in the video. We can observe that, VQ-SAM can accurately identify target-specific and background distractor regions in the videos, which are used to enhance the discriminability of evolved memory.



Fig. 9: Selected target and distractor cues from the video.

S5.5 Comparison of Attention Maps

To analyze the efficacy of our memory evolution for visual query localization, we show the attention maps in the memory attention module with and without using our approach in Fig. 10. From Fig. 10, we can see that, our method with memory evolution using target and distractor cues is able to better focus on queried target in the video, leading to better localization and segmentation performance.

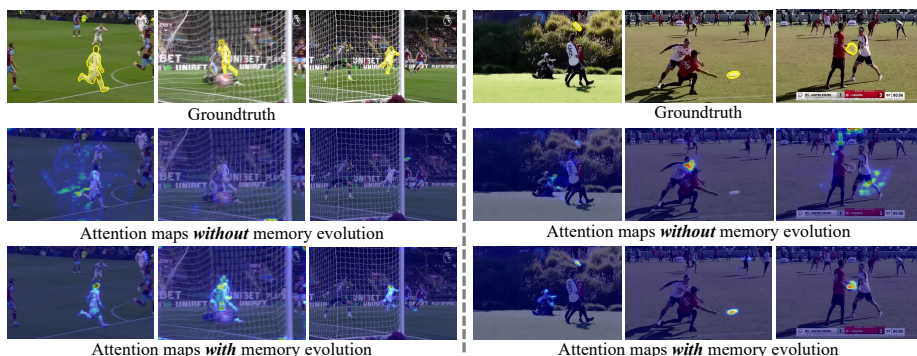


Fig. 10: Comparison of attention maps with and without memory evolution. From this figure, we can clearly observe that the attention maps of with memory evolution can better focus on the target object for segmentation and localization.



Fig. 11: Qualitative results of our VQ-SAM and representative methods.

S5.6 Qualitative Results

In order to provide further analysis of our VQ-SAM, we demonstrate the qualitative results of its segmentation and compare VQ-SAM against representative methods in Fig. 11. From the shown visualizations in Fig. 11, other methods struggle to locate and segment the target object accurately in the video. In contrast, our VQ-SAM successfully segments the target across frames, showing the efficacy of memory evolution and spatial-temporal modeling in our approach.

S6 Ethical Statement and Maintenance of VQS-4K

Ethical Statement. The construction of VQS-4K strictly follow ethical standards. All video sequences are collected under the *Creative Commons* license, and are used for *research purpose only*. However, we understand that the license of certain videos may change in the future. Once any notification of the change of video licenses is received, we will take appropriate actions to handle it.

Maintenance. VQS-4K will be hosted on the popular Github, which allows us to conveniently check feedback for improving VQS-4K via necessary maintenance. Besides, all experimental results of compared approaches and our VQ-SAM on VQS-4K will be released. Our ultimate goal is to offer a long-term and stable platform to foster research on visual query segmentation.

References

1. Carion, N., Gustafson, L., Hu, Y.T., Debnath, S., Hu, R., Suris, D., Ryali, C., Alwala, K.V., Khedr, H., Huang, A., et al.: Sam 3: Segment anything with concepts. In: ICLR (2026) [11](#), [12](#)
2. Chang, J., Hong, S., Lee, H., Ha, S.J., Lee, D., Kim, S.T., Choi, J.: Hero-vql: Hierarchical, egocentric and robust visual query localization. In: BMVC (2025) [1](#), [4](#)
3. Cheng, H.K., Oh, S.W., Price, B., Lee, J.Y., Schwing, A.: Putting the object back into video object segmentation. In: CVPR (2024) [4](#), [11](#), [12](#)
4. Cheng, H.K., Schwing, A.G.: Xmem: Long-term video object segmentation with an atkinson-shiffrin memory model. In: ECCV (2022) [4](#)
5. Deng, J., Dong, W., Socher, R., Li, L.J., Li, K., Fei-Fei, L.: Imagenet: A large-scale hierarchical image database. In: CVPR (2009) [5](#)
6. Ding, H., Liu, C., He, S., Jiang, X., Torr, P.H., Bai, S.: Mose: A new dataset for video object segmentation in complex scenes. In: ICCV (2023) [2](#), [4](#), [6](#)
7. Ding, S., Qian, R., Dong, X., Zhang, P., Zang, Y., Cao, Y., Guo, Y., Lin, D., Wang, J.: Sam2long: Enhancing sam 2 for long video segmentation with a training-free memory tree. In: ICCV (2025) [11](#), [12](#)
8. Fan, B., Feng, Y., Tian, Y., Liang, J.C., Lin, Y., Huang, Y., Fan, H.: Prvql: Progressive knowledge-guided refinement for robust egocentric visual query localization. In: ICCV (2025) [1](#), [3](#), [4](#), [11](#), [12](#), [14](#)
9. Grauman, K., Westbury, A., Byrne, E., Chavis, Z., Furnari, A., Girdhar, R., Hamburger, J., Jiang, H., Liu, M., Liu, X., et al.: Ego4d: Around the world in 3,000 hours of egocentric video. In: CVPR (2022) [1](#), [2](#), [3](#), [5](#), [6](#), [7](#), [14](#)
10. Hong, L., Chen, W., Liu, Z., Zhang, W., Guo, P., Chen, Z., Zhang, W.: Lvos: A benchmark for long-term video object segmentation. In: ICCV (2023) [2](#), [4](#), [6](#)
11. Jiang, H., Ramakrishnan, S.K., Grauman, K.: Single-stage visual query localization in egocentric videos. In: NeurIPS (2023) [1](#), [4](#), [11](#), [12](#), [14](#)
12. Khosla, S., Schwing, A., Hoiem, D., et al.: Relocate: A simple training-free baseline for visual query localization using region-based representations. In: CVPR (2025) [1](#), [4](#), [14](#)
13. Khosla, S., TV, S., Lee, B., Schwing, A., Hoiem, D.: Ren: Fast and efficient region encodings from patch-based image encoders. In: NeurIPS (2025) [1](#), [4](#), [11](#), [12](#), [14](#)
14. Lee, S., Seo, J., Choi, M., Han, K., Jeong, J., Durante, Z., Adeli, E., Park, S.H., Im, S.: Lomm: Latest object memory management for temporally consistent video instance segmentation. In: ICCV (2025) [11](#), [12](#)
15. Lin, T.Y., Dollár, P., Girshick, R., He, K., Hariharan, B., Belongie, S.: Feature pyramid networks for object detection. In: CVPR (2017) [11](#)
16. Liu, Q., Wang, J., Yang, Z., Li, L., Lin, K., Niethammer, M., Wang, L.: Livos: Light video object segmentation with gated linear matching. In: CVPR (2025) [4](#)
17. Loshchilov, I., Hutter, F.: Decoupled weight decay regularization. In: ICLR (2019) [11](#)
18. Manigrasso, Z., Dunnhofer, M., Furnari, A., Nottebaum, M., Finocchiaro, A., Marana, D., Forte, R., Farinella, G.M., Micheloni, C.: Online episodic memory visual query localization with egocentric streaming object memory. In: WACV (2026) [1](#), [4](#)
19. Oh, S.W., Lee, J.Y., Xu, N., Kim, S.J.: Video object segmentation using space-time memory networks. In: ICCV (2019) [4](#)

20. Paszke, A., Gross, S., Massa, F., Lerer, A., Bradbury, J., Chanan, G., Killeen, T., Lin, Z., Gimelshein, N., Antiga, L., et al.: Pytorch: An imperative style, high-performance deep learning library. In: NeurIPS (2019) [11](#)
21. Peng, L., Gao, J., Liu, X., Li, W., Dong, S., Zhang, Z., Fan, H., Zhang, L.: Vast-track: Vast category visual object tracking. NeurIPS (2024) [5](#)
22. Perazzi, F., Pont-Tuset, J., McWilliams, B., Van Gool, L., Gross, M., Sorkine-Hornung, A.: A benchmark dataset and evaluation methodology for video object segmentation. In: CVPR (2016) [2](#), [4](#)
23. Qi, J., Gao, Y., Hu, Y., Wang, X., Liu, X., Bai, X., Belongie, S., Yuille, A., Torr, P.H., Bai, S.: Occluded video instance segmentation: A benchmark. International Journal of Computer Vision **130**(8), 2022–2039 (2022) [4](#)
24. Qin, G., Wang, Z., Shen, D., Liu, H., Zhou, H., Wu, J., Hu, R., Jin, Y.: Structure matters: Revisiting boundary refinement in video object segmentation. In: ICCV (2025) [4](#), [11](#), [12](#)
25. Ravi, N., Gabeur, V., Hu, Y., Hu, R., Ryali, C., Ma, T., Khedr, H., Rädle, R., Rolland, C., Gustafson, L., Mintun, E., Pan, J., Alwala, K.V., Carion, N., Wu, C., Girshick, R.B., Dollár, P., Feichtenhofer, C.: Sam 2: Segment anything in images and videos. In: ICLR (2025) [3](#), [4](#), [8](#), [9](#), [10](#), [11](#), [12](#)
26. Ryali, C., Hu, Y.T., Bolya, D., Wei, C., Fan, H., Huang, P.Y., Aggarwal, V., Chowdhury, A., Poursaeed, O., Hoffman, J., et al.: Hiera: A hierarchical vision transformer without the bells-and-whistles. In: ICML (2023) [11](#)
27. Vaswani, A., Shazeer, N., Parmar, N., Uszkoreit, J., Jones, L., Gomez, A.N., Kaiser, L., Polosukhin, I.: Attention is all you need. In: NIPS (2017) [9](#)
28. Videnovic, J., Lukezic, A., Kristan, M.: A distractor-aware memory for visual object tracking with sam2. In: CVPR (2025) [3](#), [10](#), [11](#), [12](#)
29. Wang, J., Zhang, P., Chu, T., Cao, Y., Zhou, Y., Wu, T., Wang, B., He, C., Lin, D.: V3det: Vast vocabulary visual detection dataset. In: ICCV (2023) [5](#)
30. Wu, Q., Yang, T., Wu, W., Chan, A.B.: Scalable video object segmentation with simplified framework. In: ICCV (2023) [4](#)
31. Xu, M., Li, Y., Fu, C.Y., Ghanem, B., Xiang, T., Pérez-Rúa, J.M.: Where is my wallet? modeling object proposal sets for egocentric visual query localization. In: CVPR (2023) [1](#), [4](#)
32. Xu, N., Yang, L., Fan, Y., Yang, J., Yue, D., Liang, Y., Price, B., Cohen, S., Huang, T.: Youtube-vos: Sequence-to-sequence video object segmentation. In: ECCV (2018) [2](#), [4](#), [6](#)
33. Yan, C., Wang, H., Yan, S., Jiang, X., Hu, Y., Kang, G., Xie, W., Gavves, E.: Visa: Reasoning video object segmentation via large language models. In: ECCV (2024) [4](#)
34. Yang, L., Fan, Y., Xu, N.: Video instance segmentation. In: ICCV (2019) [2](#), [4](#)
35. Yao, J., Deng, X., Gu, X., Dai, M., Fan, B., Zhang, Z., Huang, Y., Fan, H., Zhang, L.: Omnistvg: Toward spatio-temporal omni-object video grounding. In: ICLR (2026) [5](#)